LAWRENCE
LIVERMORE
NATIONAL
LABORATORY

LLNL-JRNL-415425

Microstructure and In-Situ Observations of Undercooling of Tin Relevant to Lead-Free Solder Alloys

John Elmer, Eliot Specht, Mukul Kumar

August 7, 2009

Journal of Electronic Materials

Disclaimer

Microstructure and In-Situ Observations of Undercooling for Nucleation of β-Sn Relevant to Lead-Free Solder Alloys

By
John W. Elmer[1,3], Eliot D. Specht[2], and Mukul Kumar[1]

1. – Lawrence Livermore National Laboratory, Livermore, CA, 94550
2. – Oak Ridge National Laboratory, Oak Ridge, TN, 37831
3. – elmer1@llnl.gov

Abstract

Difficult nucleation of β-Sn during solidification of tin and tin-based lead free solder alloys can result in high degrees of undercooling of the liquid prior to solidification. The undercooling can produce solder joints with large grains, anisotropic behavior, and undesirable mechanical properties. This paper examines the amount of undercooling of tin on both graphite (non-wetting) and copper (wetting) surfaces using an *in-situ* x-ray diffraction technique. Microstructural characterization was further performed by optical microscopy, scanning electron microscopy and electron backscattering diffraction imaging microscopy. Undercoolings as high as 61ºC were observed Sn solidified on graphite, while lower undercoolings, up to 30ºC were observed for Sn solidified on copper. The microstructure of the high purity Sn sample solidified on graphite showed very few grains in the cross section, while the commercially pure Sn sample solidified with only one grain and was twinned. Tin solidified on copper contained significant amounts of copper in the tin, intermetallic phase formation at the interface, and a eutectic microstructure.

KeyWords: In-situ x-ray diffraction, solidification, nucleation, undercooling, twinning, grain boundaries, tin, lead-free solders, cooling rate, microstructure, wetting.

Introduction

Tin-based alloys represent the vast majority of solders being used as lead-free alternatives to traditional solders. These alloys are finding numerous application in everything from consumer electronics to high reliability components for military and aerospace components. This departure away from lead-containing traditional alloys is being driven not only by legislation to remove toxic metals, such as lead and cadmium, from solder and brazing alloys [1, 2], but also by a need to produce higher quality components more efficiently. Although cadmium has largely been eliminated from brazing alloys by finding suitable alternatives, lead has not been completely eliminated from solder alloys due to the wide ranging applications in the microelectronics industry.

Many of the lead-free replacement solders under consideration are based on the Sn-Ag eutectic modified with small amounts of Cu, Bi or Sb to improve strength and creep resistance while maintaining a melting point close to that of the Sn-Ag eutectic of 217ºC [3]. Other lead-free solders deviate considerably from the Sn-Ag eutectic in attempts to improve properties or intentionally change the liquidus and solidus temperatures for one reason or another, but nearly all are Sn-based alloys containing 90%Sn or more. The prevalence of Sn in lead-free solders and its increasing importance to the electronics industry requires that significant resources be devoted into understanding the fundamental properties of tin as it relates to all aspects of soldering.

Tin is unusual in that it is one of only two elemental metals with a tetragonal crystal structure and undergoes a low temperature phase transformation from α (fcc) which is an undesired phase of tin to β (bct) at 13.2ºC and above. In addition, during solidification the solid β-Sn phase is difficult to nucleate from the liquid, which results in observed undercoolings of over 100°C below its melting point under very carefully controlled conditions [4,5], and the amount of undercooling was shown to monotonically increase with decreasing solder ball size [6]. Even under normal processing conditions at moderately low cooling rates, undercoolings of up to 40ºC have been observed [4]. The undercooling results in very fast growing β-Sn dendrites, and produces a textured microstructure with few individual grains in the solder joint [7]. Under these conditions, the anisotropic nature of tetragonal β-Sn is not randomized, leading to mechanical weakness of the joint, particularly where thermal fatigue is a concern [8-10]. The unusual solidification behavior of pure tin continues into the Sn-rich solder alloys which results in undercoolings of 25-40ºC [11]. The associated formation of non-equilibrium microstructures is almost always detrimental to the mechanical properties of the resulting solder joint. Delayed nucleation of β-Sn during solidification is known to result in higher fractions of primary, or primary-like, constituents, large β-Sn dendrites, large grains, reduced amounts of eutectic, higher amounts of microconstituents, and undesired morphologies of the intermetallic compounds (e.g. large Ag_3Sn plates or long Cu_6Sn_5 needles) which are often hard and brittle [11-13].

This paper investigates the properties of tin melted and solidified on different substrates, using *in-situ* x-ray diffraction methods to directly observe the amount of undercooling prior to solidification to β-Sn. The results are combined with microstructural characterization of the solidified tin samples to show the influence of graphite (non-wetting) and copper substrates on the final microstructure.

Experimental Procedures

In-situ x-ray diffraction experiments were performed at the Advanced Photon Source (APS) using a setup similar to the one used previously to study phase transformation of metals under controlled heating and cooling conditions [14-18]. These experiments are performed by rapidly heating and cooling samples under controlled conditions while simultaneously performing x-ray diffraction in real time, using the UNICAT beam line BM-33-C at the APS with a 29.1 keV x-ray beam from a ring current of 100 mA. This energy is just below the Sn k-α absorption edge of 29.2 keV, allowing for deep penetration of the x-rays into the Sn-rich solder samples. This beam line is set up with a water cooled Si (111) monochromator, and the beam is focused and sized to dimensions of approximately 2 mm wide by 0.5 mm high using a dynamically bent Si crystal and collimator slits. A schematic illustration of the experimental setup is shown in Fig 1, and additional details about these x-ray diffraction experiments are provided elsewhere for in-situ measurements of phase transformations [15-16], diffusion [17], and stress relaxation [18].

The new experiments on tin-based solder alloys required a modification to the previous setup since the samples will be molten during a portion of time. To do this, a graphite sample holder was designed for resistive heating which in turn heats the tin alloys and metal substrates inside. A graphite sample holder was chosen since it is non-reactive with tin, and is easily heated using resistive methods. The sample holder design is shown in Fig. 2, measuring 100 mm x 8 mm x 5 mm, with a 5 mm diameter circular disk machined out of the top surface to hold the metal samples. Different hole depths were machined into the sample holder, allowing different combinations of solder alloy thicknesses and substrates to be used. A 1mm diameter hole was further drilled into the side of the graphite sample holder to allow a Type K thermocouple to be placed directly below the center of the solder disk. Silver-loaded thermally conductive grease was placed in the hole to insure good thermal contact between the thermocouple and the graphite. The experiments were performed by placing the loaded sample holder into the water cooled grips of the heating stage with a ~5 deg tilt to the axis of the x-ray beam, and aligned so that the 2 mm x 0.5 mm beam is centered on the sample. An environmental chamber was then placed over the sample and evacuated using a turbo-molecular pump to prevent oxidation of the samples during the *in-situ* experiments.

Two basic types of experiments were performed. In the first, Sn was heated to and from its melting point at different rates to observe phase transformations as a function of temperature and time. In these experiments, the tin sample was loaded directly into the graphite sample holder with its surface at the same level as that of the graphite. A Kapton strip measuring 100 mm x 8 mm x 0.100 mm was then placed over the top of the sample holder to hold the sample in place. Figure 3a illustrates this setup where the Kapton layer contains the molten tin and is thin enough to allow X-rays to pass through it. In addition, the Kapton does not react with the solder and keeps the surface flat by preventing the liquid solder from balling at its center point. The second type of experiment, the tin was placed on a Cu substrate to observe the Sn-Cu reactions. Figure 3b is a schematic illustration of the solder and substrate combination with the thin Kapton layer stretched over the top to keep the tin layer contained and flat.

The alloys used in the experiments consisted of high purity tin (99.999%Sn, Alfa Aesar #38538), commercial purity tin (99.8%Sn, Alfa Aesar #43233), high purity graphite, and high purity copper substrates. Table 1 lists the alloys and the thicknesses of each sample. Since tin readily oxidizes at room temperature, an oxide layer exists on the initial samples that prohibit them from wetting onto the copper substrate and flowing onto the graphite substrate. In order to reduce the surface oxide layer the tin samples were dipped into a rosin-based mildly active (Indium Corporation RMA Flux #5) liquid flux prior to assembling into the graphite sample holder. This flux is reported to contain 40-50% rosin mixture, 30-40% isopropol alcohol, 10-30% methyl ethyl keytone and 1-2% proprietary ingredients by weight.

Characterization of the solidified solder samples was further performed after the *in-situ* x-ray diffraction experiments using optical light microscopy, scanning electron microscopy (SEM), and electron backscattering diffraction imaging (EBSD) [19]. The samples were carefully prepared for microstructural characterization by first mounting the solder disk in two-part epoxy or silver loaded conductive epoxy. After hardening, the samples were gently hand-sanded to their ¼ radius location to reveal the cross section of the solder disk using successive grits of silicon-carbide paper. The samples were then polished using 3 micron followed by 1 micron diamond paste on an automatic polishing wheel. Optical microscopy was performed on the Sn samples solidified on graphite in the as polished condition while the Sn samples solidified on copper were etched prior to examination. The SEM and EBSD analyses were performed on polished samples using an EBSD detector mounted on a Philips XL30S FEG-SEM. The grain orientations were mapped and analyzed to determine orientation relationships in the solidified Sn samples.

Results

Tin on Graphite Substrates

The first set of experiments consisted of melting and solidifying high purity and commercial purity tin on a graphite surface, using the experimental setup that is schematically illustrated in Fig. 3a. Since graphite and Kapton do not react with tin, the tin melts and solidifies in such a way that any heterogeneous nucleation effects induced by the substrate are minimized. One would therefore expect that the amount of undercooling of the liquid tin during solidification is likely to be larger than if the tin was in contact with a reacting substrate such as copper. The tin samples were heated at a rate of 2ºC/s, held at the peak temperature of 257ºC for 1s, and then cooled at rates between 0.1 and 5ºC/s. Thus the total time spent above the liquidus temperature of tin (232ºC) was in excess of 20s in all case, which was sufficient for the tin to melt and flow to a smaller diameter disk shape under the constraining force of the Kapton cover. A time-temperature profile for one of the commercial purity Sn samples cooled at a slow rate of 0.1 ºC/s is shown in Fig.4, as measured by the thermocouple directly below the sample. The temperature profile is controlled down to approximately 125ºC, and free cooled during the remainder of the experiment.

While the sample is being heated and cooled, x-ray diffraction patterns were taken and later analyzed to determine when β-Sn first appeared, which indicates the onset of solidification. Figure 5 shows one of the initial diffraction patterns for the commercial purity Sn at room temperature. There are eight Sn diffraction peaks that appear in the x-

ray diffraction window between 1.4Å and 3.0Å. Strong graphite peaks appear at higher d-spacings (not shown). The two most prominent Sn peaks are the Sn (200) located at 2.916 Å, and the Sn (101) located at 2.793Å, as calculated from the lattice parameters of bct white Sn of a= 5.8313 Å and c=3.1815 Å [20]. Note that texturing of the thin foil alters the diffraction intensities of the peaks, and in this case, has resulted in an increase in the Sn(101) relative to the Sn (200) from the ideal powder diffraction condition. In addition, very few grains in the solidified solder samples result in even more dramatic changes in these intensities, including the disappearance of many of the peaks as will be seen later.

Figure 6 shows the results from one of the *in-situ* x-ray diffraction runs where the commercial purity tin (99.8%Sn) was melted and solidified in the graphite sample holder following the time-temperature profile shown in Fig. 4. This result shows the sequential diffractions patterns, plotted as d-spacing on the x-axis versus x-ray scan number along the y-axis, where each x-ray scan was taken at a 3s interval. The x-ray diffraction patterns are plotted in pseudocolor format, indicated by the adjacent intensity scale.

The initial diffraction pattern, scan 0, corresponds to the tin disk sitting on the graphite sample holder prior to heating the sample. A wide graphite diffraction peak (002) appears at d~3.3Å, and two Sn peaks appear at 2.75Å Sn(101), and 2.85Å Sn(200) in this figure. Once heating begins, the Sn and graphite peaks move to higher d-spacings due to lattice expansion effects, and the Sn melts at frame 32. Complete melting of the sample is characterized by the disappearance of the Sn peaks and the appearance of a more diffuse background characteristic of liquid Sn, while the graphite peak remains essentially constant throughout the experiment. Solidification began and finished at frame 275 where the Sn (200) peak reappears and remains throughout the remainder of the experiment. The absence of the Sn (101) peak on solidification indicates that the sample has few diffracting grains, as discussed below. Due to these poor grain statistics, freezing cannot be reliably detected by the appearance of Bragg reflections from the solid; the disappearance of the diffuse scattering from the liquid is a more robust indicator of freezing.

Analysis of the thermal profile for the sample indicates that it melted at 242ºC, which is 10ºC higher than the equilibrium value. This apparent superheating is related to several possible factors, including the temperature resolution of the experiment. With a heating rate of 2ºC/s, and a sampling rate of 1 sample every 3s, there is up to 6ºC uncertainty in the data, and the remaining difference is related to the accuracy of the thermocouple and temperature gradients in the sample. During cooling, solidification was indicated to occur at a temperature of 171°C, which is 61°C below its equilibrium value. This large degree of undercooling is consistent with what has been observed by others for tin solidified under careful conditions in contact with non-reacting substrates [4, 5]. We expect that the measurement of freezing temperature is more accurate than that of melting temperature, for two reasons: the sample is cooled more slowly than it is heated, giving finer temperature resolution, and the graphite sample holder is in better thermal contact with the cooling liquid Sn that with the solid Sn disk on heating.

Two other runs were made with commercially pure Sn at cooling rates of 1 and 5°C/s. These results are summarized in Table 2, showing that the average undercooling of the commercially pure Sn samples was 55°C. Note that there is no obvious trend between cooling rate and undercooling for the range of cooling rates studied. Additional

samples need to be run in order to get a statistical variation in the undercooling as a function of cooling rate, and these experiments are planned as future work.

Similar results were obtained for the high purity Sn sample (99.999%Sn) on the graphite substrate, however, the measured undercooling was not as large. In the case of high purity Sn, the sample melted at 246°C, and solidified at 212°C. This results in a 20°C undercooling below the melting point of pure Sn (232°C). This rather low undercooling was unexpected, and additional experiments are planned as future work to gather statistics on the undercooling of high purity Sn.

The measured undercooling in both the high purity and commercial purity Sn samples is high enough to confirm that nucleation of β-Sn is difficult, and that there is likely an adverse effect on the microstructure. To take a closer look at this, the microstructure of the two solidified tin disks was characterized using optical light microscopy on metallographically sectioned and polished samples. Fig. 7a shows the microstructure near the half-radius location of the solidified high purity Sn disk, where the microstructure is characterized by having very few grains. This sample was originally in the form of a 5 mm diameter disk, 50 μm thick, and after solidification has become thicker. Bumps in the surface correspond to the flux was trapped between the Sn and the substrate. The grain boundaries are clearly defined by light and dark contrast in the polarized light, and are wavy in appearance.

To better understand the microstructures of the solidified tin samples, EBSD was used to characterize the nature of the grain boundaries and other features. Figure 7b shows an EBSD inverse pole figure shows the results for the high purity Sn sample solidified on graphite, which contained only a few grains in the cross section. These results show the same large angle grain boundaries that are observed by optical microscopy, but also indicate substructure within these grains. The substructure is indicated by changes in the color shading and are particularly evident in the grain marked ‘b’, which is near the (001) corner of the stereographic triangle. The misorientation within the grains of the microstructure is shown in Fig. 8a for a grain that showed only slight variations in misorientation, and in Fig. 8b for a grain that showed a larger variation in misorientation. The misorientation plot shown in Fig. 8a corresponds to the scan marked ‘a’ in the EBSD map shown in Fig. 7b, and plots the misorientation as both a point-to-point and a cumulative point-to-origin trace. The misorientation in this sample is small, showing point-to-point variations on the order of 1°or less, and the cumulative misorientation is only 2° over the 120 μm trace. For the EBSD scan marked ‘b’ in Fig. 7b, larger misorientations are present, up to 4°, with point-to-point variations occurring on the 5 μm scale.

The microstructures of the commercial purity Sn samples solidified on graphite are shown in Fig. 9 for solidification rates of 0.1 and 1ºC/s. These microstructures are considerably different than those of the high purity Sn samples. In Fig. 9a, the microstructure of the more slowly cooled commercially pure Sn sample is completely featureless, except for what appears to be several twins in the upper right hand corner. In Fig. 9b, the microstructure of the more rapidly cooled sample is still different, having a candy-striped appearance with alternating light and dark bands that have an angular appearance running completely across the sample. In both cases, the commercially pure Sn samples are believed to have solidified as one grain prior to twinning that occurred during cooling as will be discussed later.

The EBSD results of the commercially pure Sn sample solidified on graphite at 1ºC/s are shown in Fig 10, which is the sample that contains a regular array of angular boundaries. The figure on top is an image quality map showing the general microstructure with the high angle boundaries, and is similar in appearance to the optical light microscopy image shown in Fig. 9b. The same area is then colored according to the inverse pole figure for each grain orientation, as shown in the lower image. The colors in the orientation map are keyed to the 001-110-110 fundamental zone for a tetragonal lattice. Table 3 summarizes the orientation relationships for the labeled grains (A-E) in Fig. 10. It can be readily seen that numerous Sigma-3 (~60°) and c-axis (~90°) twin orientations nucleated within the big grain that is labeled "A". Here it is clear that there are two major grain orientations corresponding to the striping of the sample, and a third orientation which traverses the stripes in two locations. The predominance of the two major orientations throughout the entire cross section of the sample indicates that the sample most likely solidified as a single grain which later transformed into the two dominant twinned grain orientations. A misorientation angle of approximately 60º is a common twinning angle for Sn [21], and the EBSD results show that the four analyzed 60º boundaries had an average misorientation of 61.8º, which is indicative of (301)[-103] twins rotated around the [010] axis [22].

The commercially pure Sn sample that was most heavily twinned was analyzed in further detail to determine if any additional information could be gained from the x-ray diffraction patterns that might be an indication of twinning. Figure 11a shows the initial diffraction pattern for this sample, which is textured such that the Sn(101) is again more intense than the Sn(200). The corresponding series of diffraction patterns for this sample are shown in Fig. 11b, from the beginning to the end of the experiment. Heating begins at t= 105s and the Sn peaks move to higher d-spacings as the sample heats up. Melting occurs at t=204s and the sample shows only diffraction from the graphite sample holder until t=286s where solidification occurs and the Sn(101) peak appears. The temperature at this point is 172ºC, and the Sn(101) peak remains to room temperature.

Individual peak analysis was performed on this data by measuring the intensity, width, and d-spacing of the Sn(101) peak after solidification occurred. These results are presented in Fig. 12, which indicate that both the peak intensity and peak width experience a sharp decrease at approximately 80ºC, while the d-spacing of the Sn(101) peak continues its approximate linear decreasing trend with temperature. From the slope of the d-spacing versus temperature plot (Fig. 12c) the contraction of Sn(101) planes was determined to be 37.0×10^{-6}/ºC based on a linear fit through the data. This value is close to the reported value for β-Sn(101) of 27.6×10^{-6}/ºC at 30ºC, and 37.6×10^{-6}/ºC at 150ºC [23]. The linear trend of the measured CTE during cooling of this sample suggests that there is no phase change occurring at 80ºC that would be responsible for the changes in peak intensity and peak width. This further suggests that the twinning is probably responsible for the observed changes in x-ray diffraction peak character at approximately 80ºC, since β-Sn would remain after twinning. The decrease in peak width would indicate that microstrains building up in the resolidified Sn disc during cooling to 80ºC are being relieved by twinning and producing more narrow diffraction peaks. In addition, the formation of newly twinned grains with different crystallographic orientations is likely contributing to the decrease in the overall observed peak intensity.

High Purity Sn on Copper Substrates

High purity Sn was melted and solidified on a Cu substrate to see how the Sn reaction with the substrate affects the microstructure and undercooling. Since Sn and copper form a eutectic at 227ºC, the tin should start to react with the Cu substrate at this temperature, which is below the melting point of Sn. Table 2 summarizes the results of three runs where high purity Sn was melted with a heating rate of 2ºC/s, and solidified on the Cu substrate at cooling rates of 4, 0.5, and 0.05ºC/s. The measured melting points were indeed lower than the melting point of pure Sn, averaging 221ºC, indicating that the Sn was reacting with the Cu substrate as expected, within the expected accuracy of the temperature measurements. These samples also displayed undercooling prior to solidification during cooling, where the amount of undercooling varied from 22ºC to 30ºC, but again having no obvious trend with cooling rate. These data are summarized in Table 2 showing an average undercooling of 26ºC below the Sn-Cu eutectic of 227ºC.

The microstructure of the Sn melted on Cu is quite different than that melted on graphite due to dissolution of Cu in liquid Sn. Figure 13 shows a cross section through one of the samples that was cooled at a rate of 0.5ºC/s, showing the intermetallic layer that forms between the Cu and the Sn. Occasional second-phase particles of in size appear in the matrix, and are approximately 3 μm in size. These particles are presumably Cu_6Sn_5, which forms during solidification of the eutectic microconstituent that occurs at 99.3 wt% Sn [24]. The intermetallic layer that formed between the Cu and the Sn has a scalloped appearance, characteristic of the Cu_6Sn_5 phase [25], and is approximately 7 μm thick. The thickness of this layer is the direct result of the long time (approximately 2 min) that the liquid Sn was in contact with the Cu substrate at the slow cooling rate of 0.5ºC/s for this sample.

EBSD imaging was further performed on the high purity Sn sample solidified on the copper substrate. Figure 14 shows the EBSD results near the center of the optical micrograph shown in Fig. 13. In the EBSD results shown in Fig. 14 the copper substrate is located in the lower half of the image and the reflowed Sn is on top. The EBSD map of the copper grains indicates the presence of large angle grain boundaries, with average grain sizes on the order of 10 μm. The interface between the Cu and the Sn shows up as a band approximately 10 μm wide with an irregular structure surrounding the Cu_6Sn_5 intermetallic phase (black shading). The reflowed Sn reacted with the copper substrate to form a large fraction eutectic constituent composed of Sn and Cu_6Sn_5 phases. The presence of the eutectic constituent results in the mottled appearance of the EBSD pattern as the different phases of the eutectic are probed by the beam. Longer vertical boundaries are also present, indicating that the Sn-Cu alloy solidified with columnar grains oriented approximately perpendicular to the Cu substrate surface. The results of these EBSD observations indicate that the Sn reflowed on the Cu substrate formed a significantly different microstructure than the Sn solidified on graphite, with a microstructure consisting of a large fraction of eutectic microconstituent, columnar grains and no twins. This microstructure formed with less undercooling than the Sn solidified on graphite and would be expected to have significantly different properties than the Sn solidified on graphite.

Conclusions

1. In-situ x-ray diffraction patterns of Sn that was melted and solidified on a non-reacting graphite substrate showed undercoolings as high as 60ºC. Differences in the purity of the Sn produced substantially different undercoolings, with less pure Sn exhibiting higher undercoolings (ΔT=55ºC) than high purity Sn (ΔT=20ºC). Due to the statistical nature of β-phase nucleation during undercooling, more samples need to be tested to confirm these results.
2. Optical metallographic examination of the highly undercooled Sn samples on graphite surfaces showed that the Sn solidified with very few grains in the microstructure. The high purity Sn sample had grains with wavy boundaries, while the commercial purity Sn samples solidified with only one grain and contained twins.
3. EBSD performed on the commercial purity Sn sample cooled on graphite showed that the tin solidified as one large grain, which later twinned with a predominant twinning angle of 61.8º. Twinning of the commercial purity Sn samples was considerably more prominent in the more rapidly cooled sample at 1ºC/s. A strong decrease in the diffraction peak width and intensity of this sample that occurred at approximately 80ºC was attributed to twinning occurring at this temperature during cooling.
4. EBSD performed on the high purity Sn sample solidified on graphite resulted in a microstructure containing large grains with wavy boundaries. No twinning was observed in this sample and the undercoolilng was less than that of the commercially pure Sn sample solidified on graphite at 20ºC.
5. In-situ x-ray diffraction of high purity Sn that was melted and solidified on a Cu substrate showed that the sample melted near the Cu-Sn eutectic of 227ºC, and solidified with less undercooling (ΔT=26ºC). The microstructure consisted of a mostly eutectic microstructure of Sn and Cu_6Sn_5 phases, with some primary Sn phase and occasional second-phase particles. Intermetallic phase formation at the interface had the appearance of Cu_6Sn_5 and was approximately 7 μm thick.
6. EBSD of the high purity Sn sample solidified on a copper substrate showed that the microstructure consisted of large columnar grains growing approximately normal to the Cu substrate. In a 10 μm band about the Cu/Sn interface, the microstructure is highly irregular, consisting of the Cu_6Sn_5 intermetallic phase, eutectic, and fine grained copper.
7. We have shown that *in-situ* x-ray diffraction can measure the large undercooling which results in a microstructure which is unsuitable for soldering applications. Future work will analyze the effects of compositional modifications on this undercooling in order to understand the mechanisms by which soldering behavior may be improved.

Acknowledgement

The authors would like to thank Mr. Jackson Go of LLNL for performing the optical metalllography, Mr. Edwin Sedillo of LLNL for performing SEM and EBSD characterization, Mr. Mike Santella of ORNL for assisting with the x-ray diffraction analysis software, and Jenia Karapetrova of the APS for assisting with the synchrotron beam-line setup and operation. This work performed under the auspices of the U.S. Department of Energy by Lawrence Livermore National Laboratory under Contract DE-AC52-07NA27344 and by Oak Ridge National Laboratory under Contract DE-AC05-00OR22725. Much of this work was supported by DOE, Office of Basic Energy Sciences, Division of Materials Science and Engineering. In-Situ experiments were performed on 34-BM-C at the APS, which is supported by the U.S. DOE, Basic Energy Sciences, Office of Science under contract No. W-31-109-ENG-38.

References

1) P. T. Vianco, "Environmental Mandates and Soldering Technology: The Path Forward," *Welding Journal*, 86(9), p. 27, 2007.
2) P. Baskin, "Challenges in Attaining Lead-Free Solders," *Welding Journal*, 86(3), p.58, 2007.
3) Handbook of Lead-Free Solder Technology for Microelectronic Assemblies, by K. J. Puttlitz and K. A. Stalter, CRC Press, 2004.
4) J. H. Perepezko, "Nucleation of Undercooled Liquids," *Materials Science and Engineering,* V65, p. 125, 1984.
5) D. Swenson, "The Effects of Suppressed Beta-Tin Nucleation on the Microstructural Evolution of Lead-Free Solder Joints," *J. Materials Science: Mater Electron*, v18, p. 39, 2007.
6) R. Kinyanjui, L. P. Lehman, L. Zavalij, and E. Cotts, "Effect of Sample Size on the Solidification Temperature and Microstructure of SnAgCu Near Eutectic Alloys," *J. Mater. Res.,* v20(11), pp 2914-2918, 2009.
7) L. P. Lehman et al, "Growth of Sn and Intermetallic Compounds in Sn-Ag-Cu Solder," *J. Electronic Materials*, v 33(12), pp 1429-14, 39, 2004.
8) K. N. Subramanian, J. G. Lee, "Effect of Anisotropy of Tin on Thermomechanical Behavior of Solder Joints," *Journal of Materials Science, : Materials in Electronics*, v15, pp 235-240, 2004.
9) T. R. Bieler, H. Jiang, L. P. Lehman, T. Kirkpatrick, and E. J. Cotts, "Influence of Grain Size and Orientation on the Thermomechanical Response and Reliability of Pb-free Solder Joints," *Proceedings of the 56th Electronic Components and Technology Conference*, pp 1462-1467, 2006.
10) D. W. Henderson, J. J. Woods, T. Goselin, A. Sarkhel, S. K. Kang, W.-K. Choi, D. –Y. Shih, C. Goldsmith, and K. J. Puttlitz, "The Microstructure of Sn in Near-Eutectic Sn–Ag–Cu Alloy Solder Joints and its Role in Thermomechanical Fatigue," *J. Mater. Res.,* v19, pp. 1608-1612, 2004.
11) D. W. Henderson, T. Gosselin, A. Sarkhel, S. K. Kang, W. K. Choi, D. Y. Shih, C. Goldsmith, and K. J. Puttlitz, "Ag_3Sn plate formation in the solidification of near ternary eutectic Sn–Ag–Cu alloys," *J. Mater. Research*, V19, p. 1608, 2004.
12) A. LaLonde, D. Emelander, J. Jeannette, C. Larson, W. Rietz, D. Swensen, D. W. Henderson, "Quantitative Metallography of Beta-Tin Dendrites in Sn-3.8Ag-0.7Cu BGA Solder Balls via EBSD and Polarized Light Microscopy," *J. Electronic Materials,* V33(12), p. 1545, 2004.
13) J. W. Elmer, T. A. Palmer and E. D. Specht, "Direct Observations of Sigma Phase Formation in Duplex Stainless Steels Using In-Situ Synchrotron X-Ray Diffraction," *Metallurgical and Materials Transactions A*, 38A(3), pp 464-475, 2007.
14) J. W. Elmer, T. A. Palmer and E. D. Specht, "In-Situ Observations of Sigma Phase Dissolution in 2205 Duplex Stainless Steel Using Synchrotron X-Ray Diffraction," *Materials Science and Engineering A*, 459 (1-2), pp151-155, 2007.
15) J. W. Elmer, T. A. Palmer, S. S. Babu, and E. D. Specht, "In-situ Observations of Lattice Expansion and Transformation Rates of α and β Phases in Ti-6Al-4V," *Materials Science and Engineering A*, 391, pp104-113, January, 2005.

16) J. W. Elmer, T. A. Palmer and E. D. Specht, "Direct Observations of Rapid Diffusion of Cu in Au Thin Films using In-Situ X-Ray Diffraction," *Journal of Vacuum Science and Technology-A*, 24(4) July/Aug, pp. 978-987, 2006.
17) J. W. Elmer, T. A. Palmer, S. S. Babu and E. D. Specht,"Low Temperature Relaxation of Residual Stress in Ti-6Al-4V," *Scripta Materialia,* v52, pp1051-1056, 2005.
18) Electron Backscatter Diffraction in Materials Science, edited by AJ Schwartz, M Kumar, and BL Adams, Kluwer Academic/Plenum Publishers (New York), 2000.
19) Pearson's Handbook of Crystallographic Data for Intermetallic Phases, desk edition, Vol. 2, *ASM International*, 1997.
20) F. Yang and J. C. M. Li, "Deformation behavior of tin and some tin alloys," *J. Mater Sci.: Mater Electron*, V18, p. 191, (2007).
21) J. Sylvestre and A. Blander, "Large-Scale Correlations in the Orientation of Grains in Lead-Free Solder Joints," *J. Electronic Materials*, V37(10), p. 1618, 2008.
22) V. T. Deshpande and D. B. Sirdeshmukh, "Thermal Expansion of Tetragonal Tin," *Acta Cryst.,* 14, pp. 355-356, 1961.
23) Binary Alloy Phase Diagrams, Second edition, Vol.2, ASM International, 1990.
24) J. O. Suh, K. N. Tu, and N. Tamura," Preferred orientation relationship between Cu_6Sn_5 scallop-type grains and Cu substrates in reactions between molten Sn-based solders and Cu," *J. Applied Physics*, V120, 063511, 2007.

Tables

Table 1: Tin and SAC solder alloys and substrates used in the experiments. Tm corresponds to the equilibrium melting temperature.

Alloy (wt%)	Composition (wt%)	Thickness (μm)	Tm (°C)
Sn-commercial purity	99.8 Sn	250	232
Sn-high purity	99.999 Sn	50	232
Cu substrate	99.95 Cu	250	1083
Graphite substrate (ISO 63 fine grained)	99.9 C	5000	3642

Table 2: Summary of measured melt and solidification temperatures, and undercooling (ΔT) of the tin on graphite and copper substrates. T^om refers to the melting point of pure Sn (232ºC) for the samples solidified on graphite and the Sn-Cu eutectic (227ºC) for the samples solidified on Cu. The heating rate was 2ºC/s on all samples.

Alloy	Substrate	Cooling Rate	Melt	Solidify	$\Delta T = (T^o m - Ts)$
		(ºC/s)	(ºC)	(ºC)	(ºC)
Sn 99.999	Graphite	2	245.9	212.0	20.0
Sn 99.8	Graphite	5	255.6	186.4	45.6
		1	255.7	172.2	59.8
		0.1	242.0	171.1	60.9
Sn 99.99	Copper	4	223.9	201.6	25.4
		0.5	219.3	204.5	22.5
		0.05	218.0	196.9	30.1

Table 3: Grain and twin boundary misorientations. EBSD results are from the commercially pure Sn sample solidified on graphite at 1ºC/s for the boundaries (A-E) indicated in Fig. 10.

Grain Boundary	Misorientation (deg)
A→ B	61.8
A→ C	62.1
A→ D	63.1
B→ C	60.2
A→ E	81.2
B→ D	87.2
B→ E	43.7

Figures

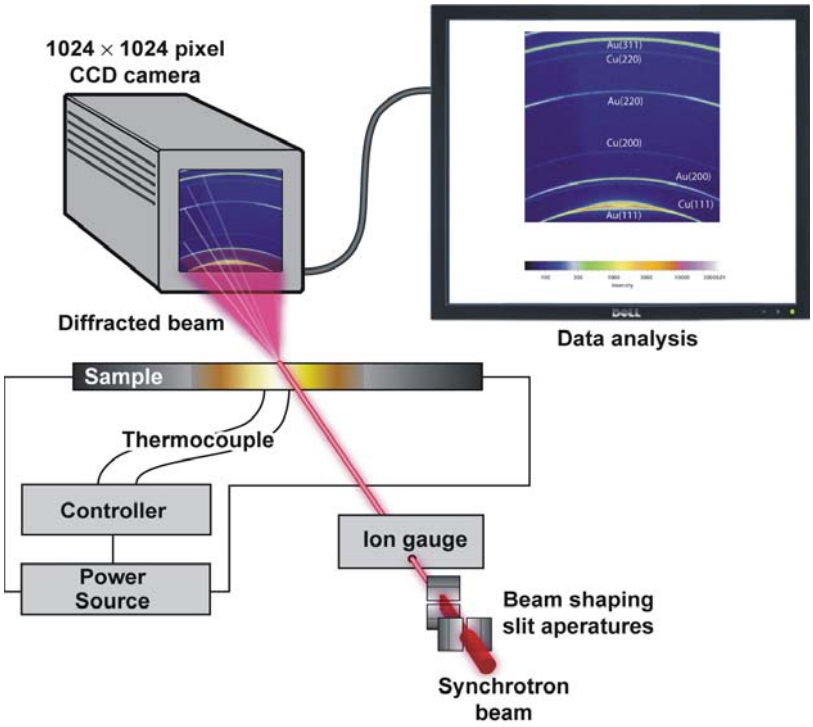

Figure 1: Schematic of the synchrotron setup for direct observations of materials being resistively heated. The sample is enclosed in an environmental chamber (not shown) to protect it from oxidation.

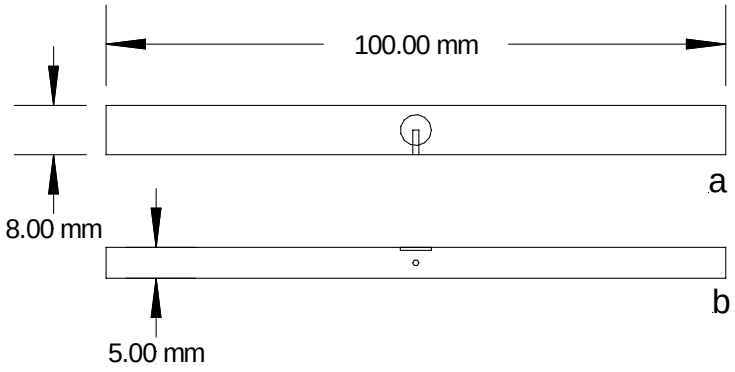

Figure 2: Graphite sample holder design a) top view, b) side view. The circular disk sample is placed in the hole (5.00 mm diameter) in the top center of the sample holder. A small hole is drilled for the thermocouple to be inserted directly below the center of the solder disk.

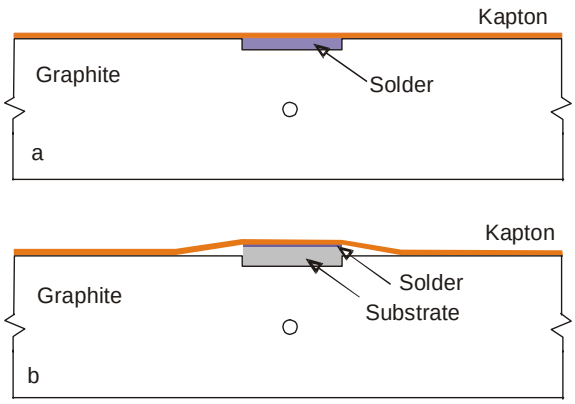

Figure 3: Schematic side-view illustrations of the graphite sample holder and solder alloy configuration for a) the Type-1 experiment where only the solder is melted and solidified in the graphite sample holder, and b) the Type-2 experiment where a thin solder layer is held in contact with a substrate.

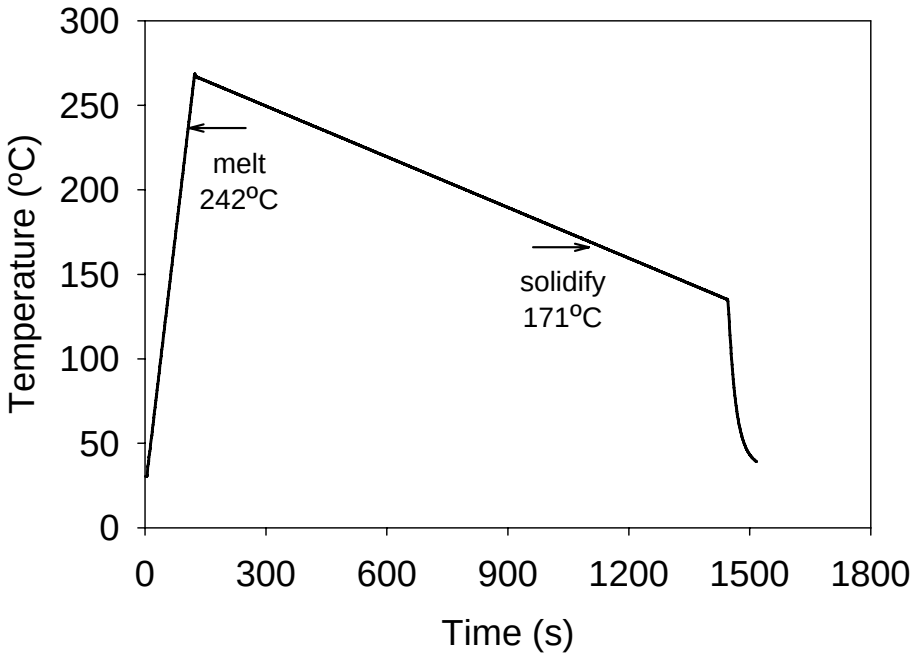

Figure 4: Time temperature profile for heating and cooling of the commercially pure Sn sample on graphite. The heating rate was 2ºC/s and the cooling rate was 0.1ºC/s over the controlled portion of the cooling curve.

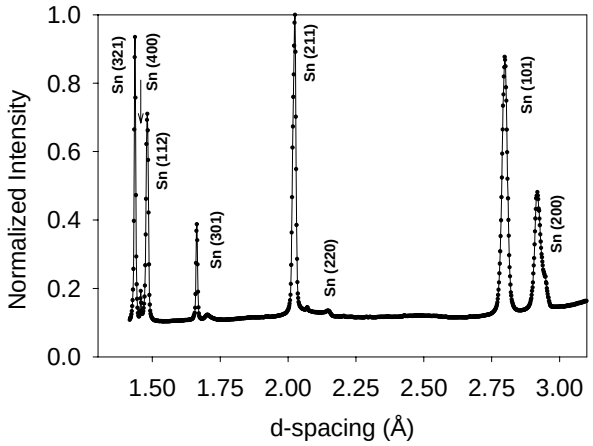

Figure 5: Initial diffraction pattern of commercial purity Sn showing the 8 Sn peaks in the diffraction window. Texture of the thin foil results in non-ideal peak intensities.

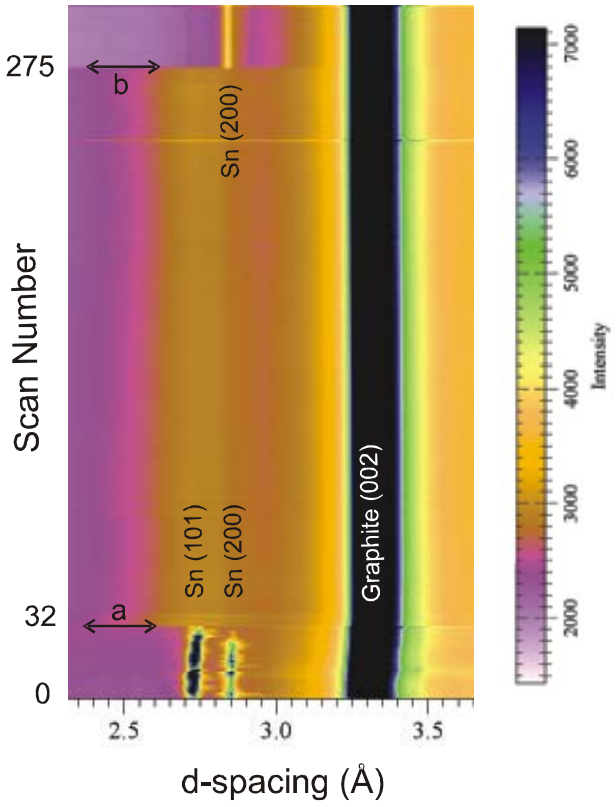

Figure 6: *In-situ* x-ray diffraction patterns for commercially pure Sn on graphite cooled at 0.1˚C/s, zoomed in to show the two major diffraction peaks of tin: Sn(101) at 2.75Å and Sn(200) at 2.85Å. The y-axis sequentially plots 300 diffraction patterns throughout the experiment. Heating begins at scan 0, melting is complete at 'a', and solidification begins and ends quickly at 'b', leaving only the Sn(200) peak diffracting during cooling.

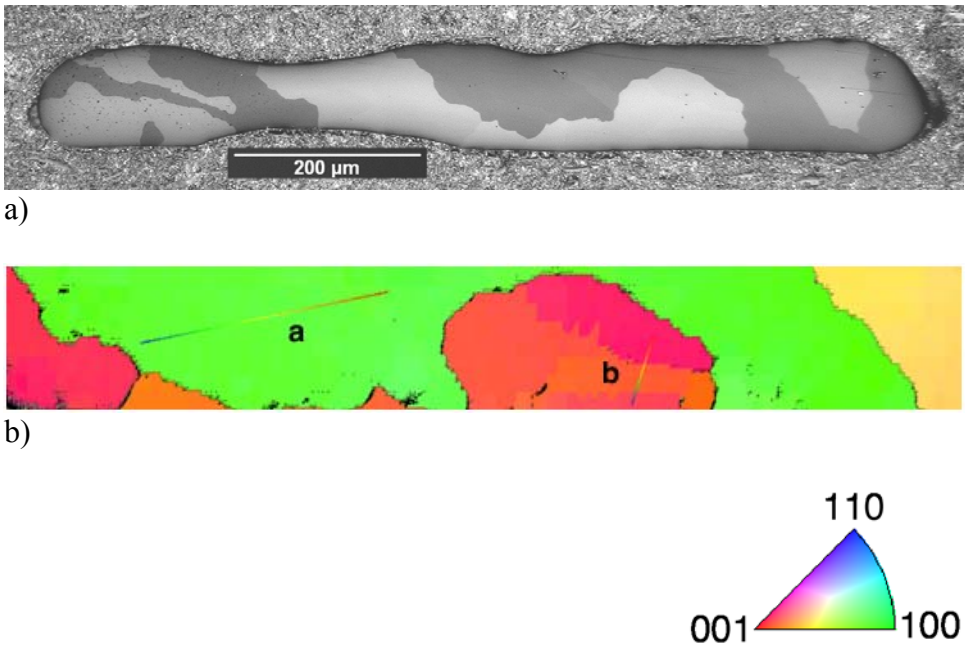

Figure 7: a) Optical light microscopy cross section through the high purity tin (99.999%Sn) sample solidified on graphite in the as polished condition using polarized light, and b) EBSD map of a portion section of the sample to the right side of center. Sample cooled at 2ºC/s.

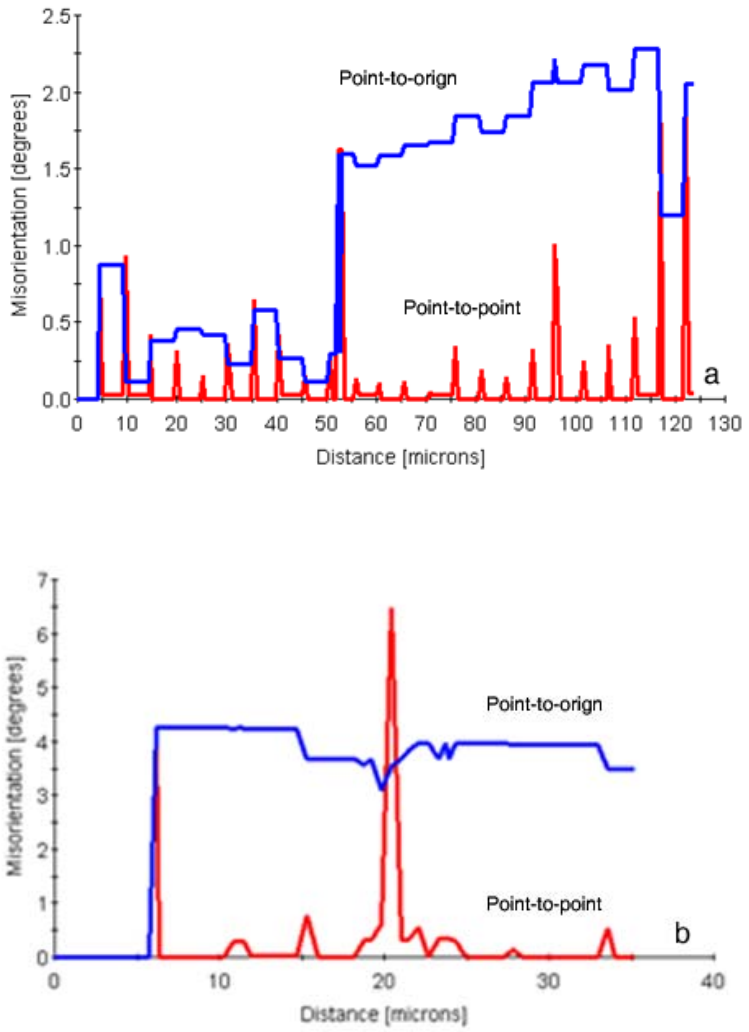

Figure 8: EBSD scans showing misorientation for in the high purity Sn solidified on the graphite surface shown in the previous figure, for a) a single grain across the scan marked ‘a’ in Fig 7b, and b) across a subgrain boundary ‘b’ in Fig. 7b.

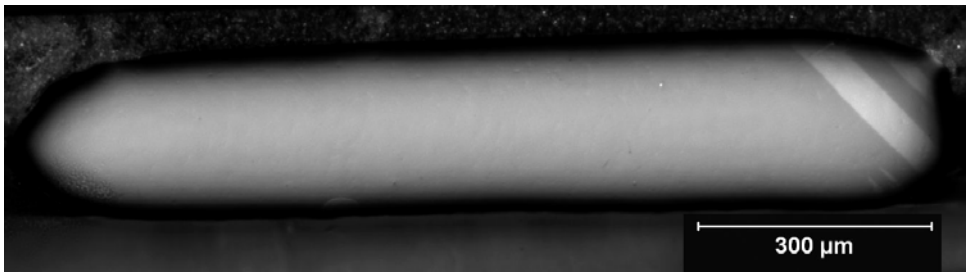

(a)

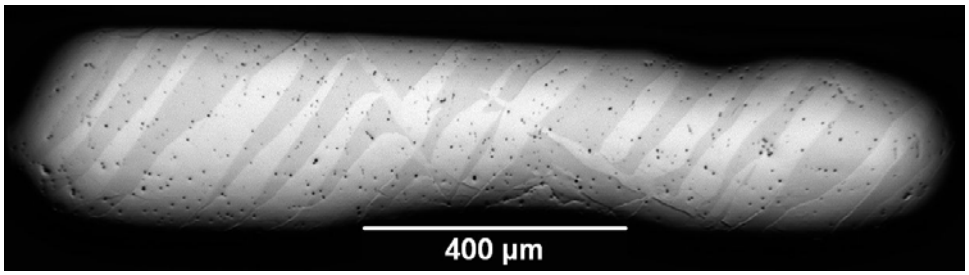

(b)

Figure 9: Optical light microscopy of the cross section through the commercially pure tin (99.8%Sn) samples in the as-polished condition using polarized light. (a) Solidified at 0.1ºC/s, and b) solidified at 1ºC/s.

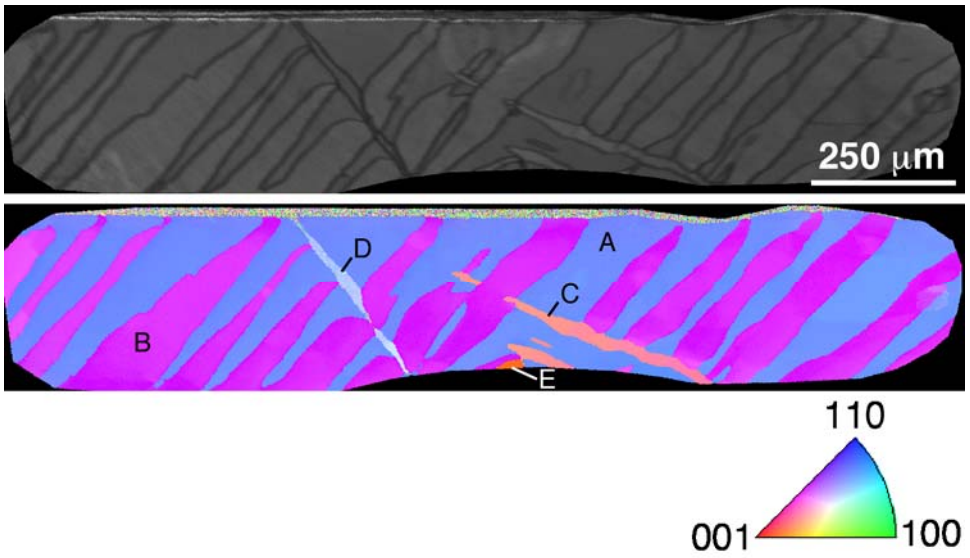

Figure 10: Results of the EBSD imaging of the grain boundaries in the commercially pure Sn solidified on the graphite surface at 1ºC/s.

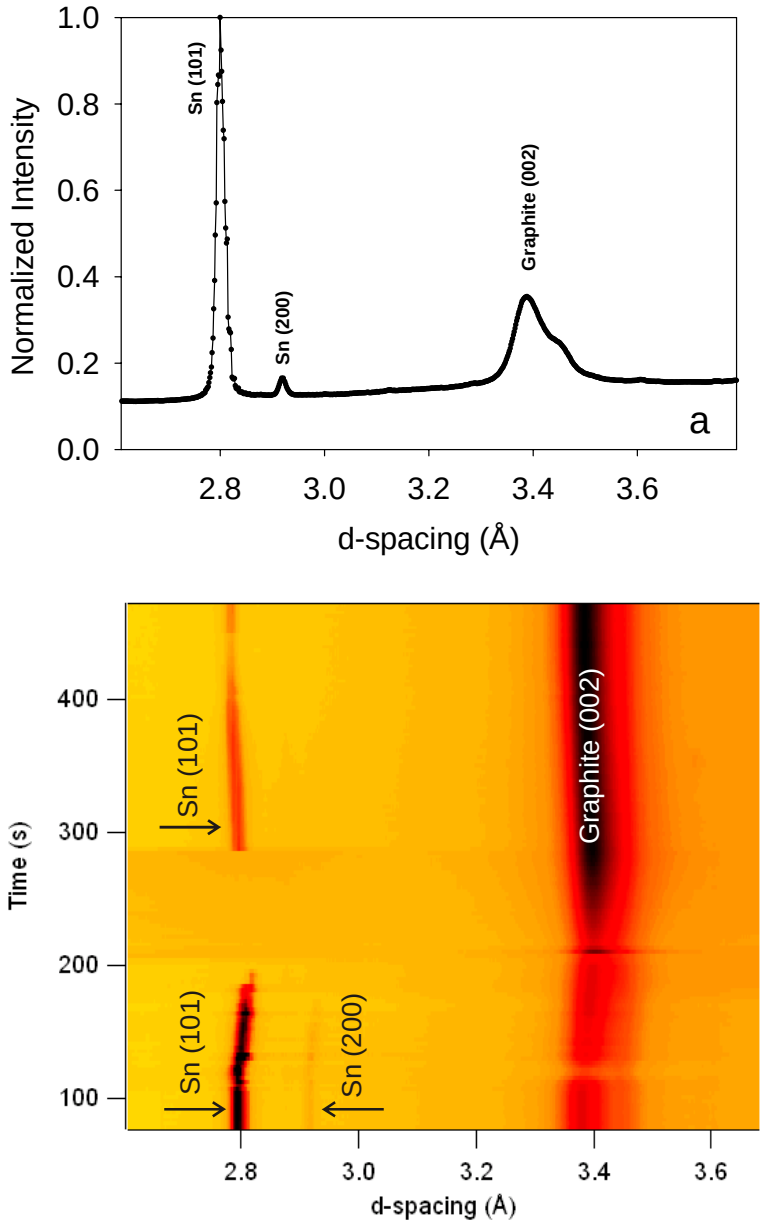

Figure 11: a) Initial diffraction peaks of the commercially pure Sn sample on graphite, prior to heating and cooling at 1˚C/s. b) In-situ x-ray diffraction patterns for heating that begins at t=105s, melting that occurs at t=204s, and solidification that begins at t= 286s. Note that the Sn(101) peak appears on solidification while the Sn(200) is absent.

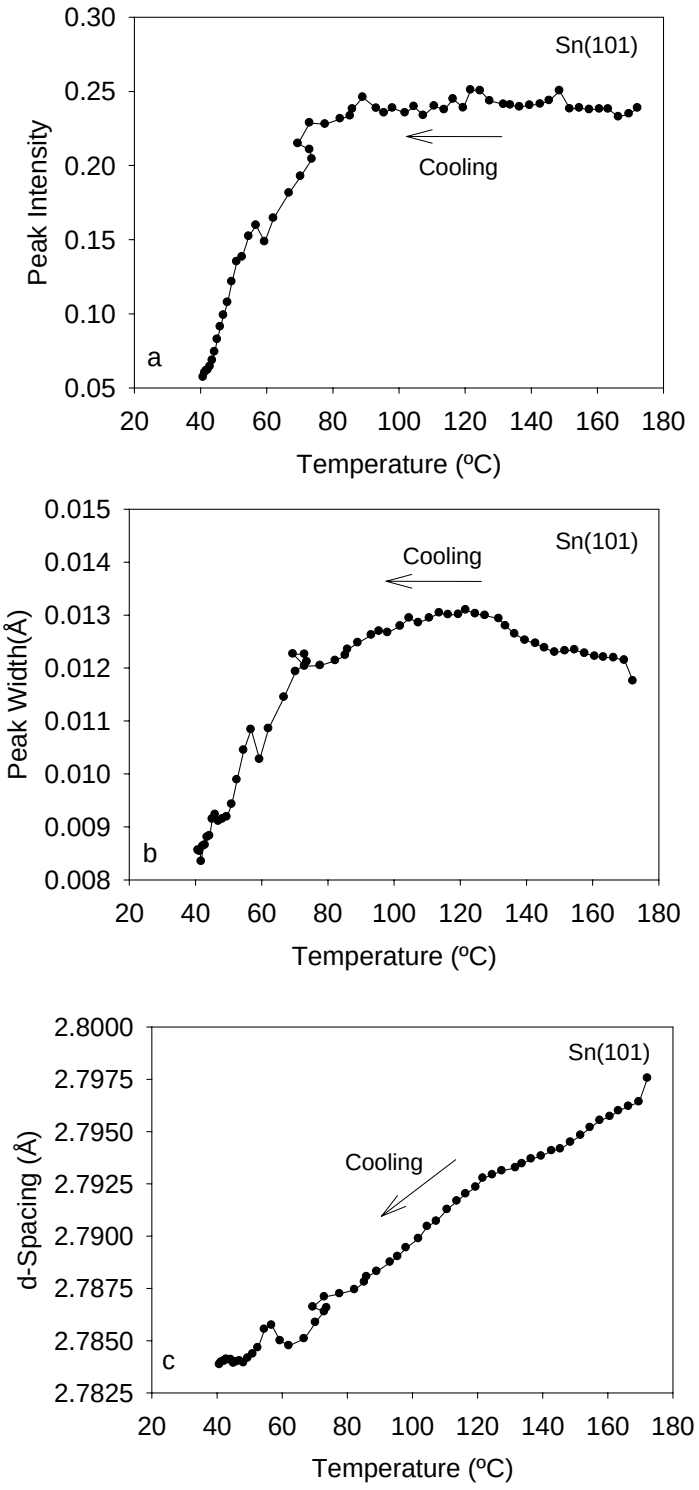

Figure 12: a) peak intensity, and b) peak width, and c) d-spacing of the Sn(101) peak during cooling of the commercially pure Sn that cooled at 1ºC/s and was heavily twinned.

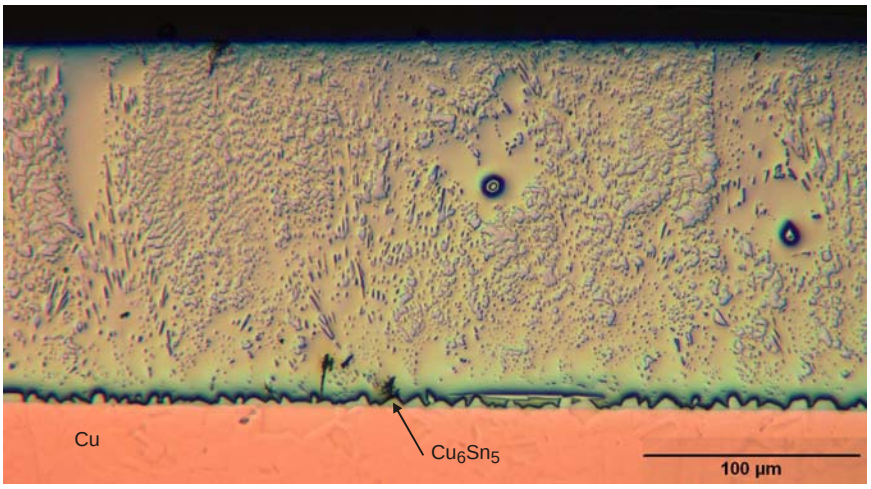

Figure 13: High purity Sn melted and solidified on a copper substrate. The low cooling rate of this sample of 0.5ºC/s allowed ample time for the liquid Sn to react with the Cu substrate.

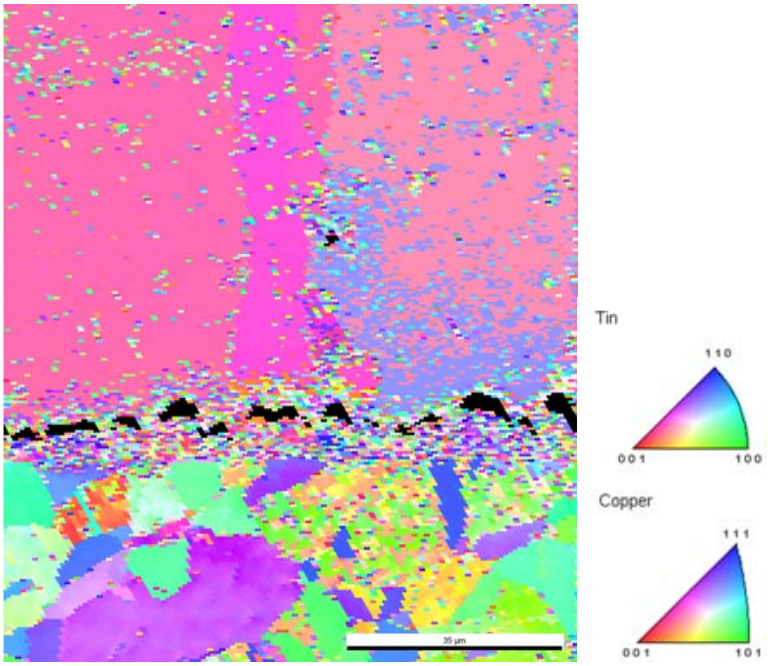

Figure 14: Results from EBSD on high purity Sn solidified on the Cu substrate. The Cu substrate is located on the lower portion of the figure and the reflowed Sn is on the upper portion of the figure.